5 March 1999

ELSEVIER

Chemical Physics Letters 301 (1999) 517–523

CHEMICAL PHYSICS LETTERS

# Photoionization mass spectrometric study of neutral species from pulsed laser ablation of $SnO_2$

S.A. Reid *

*Department of Chemistry and Center for Sensing Technology, Marquette University, P.O. Box 1881, Milwaukee, WI 53201-1881, USA*

Received 7 October 1998; in final form 1 December 1998

**Abstract**

We report the application of vacuum ultraviolet (VUV) photoionization mass spectrometry (PIMS) to probe neutral species generated in the 532 nm laser ablation of sintered $SnO_2$ targets. The major ($>90\%$) Sn containing species are of composition $(SnO)_x$ ($x = 1,2,3$), with near-natural abundance isotopic distributions. The translational energy distribution was determined for each product and compared to a Maxwellian velocity distribution. The utility of VUV PIMS as a universal probe of neutral species produced in laser ablation is discussed. © 1999 Elsevier Science B.V. All rights reserved.

## 1. Introduction

Thin films of semiconductor materials such as $SnO_2$ have important applications in, e.g., gas sensors, display systems, and solar cells [1–5]. Thin $SnO_2$ films have been grown using a variety of techniques including organometallic chemical vapor deposition (CVD) [6–9], laser-assisted CVD [10,11], spray pyrolysis [12,13], reactive-ion sputtering [14], and pulsed-laser ablation (PLA) [15–18]. The latter is particularly useful for growth of high-quality oriented films due to the facile production of highly energetic gas-phase reactants, which facilitates film growth and adhesion to the substrate (see, e.g., Ref. [19]). An important aspect of film deposition is the need to monitor the chemical composition and energetics of the ablated material in order to understand film growth processes.

Many studies have used PLA for thin-film deposition [19], and various techniques have been applied to probe both neutral and charged species in the ablated plume. These include optical spectroscopies such as optical emission spectroscopy [20], laser-induced fluorescence (LIF) [21], and resonance-enhanced multiphoton ionization (REMPI) [22], and mass spectrometry [23–29]. Optical spectroscopies are species- and state-selective but require advance knowledge of the electronic states of the species of interest and are difficult to implement for transient species with poorly known or dissociative electronic states. Mass spectrometry has been extensively applied to detect charged species [23–27]; however, at fluences typical of deposition conditions the ion product fraction is small (typically $<1\%$) [22,25], and neutral detection necessitates post-ablation ionization. Single-photon (VUV) photoionization mass spectrometry (PIMS) is an attractive method of detection for transient neutral species which to date has received little attention in PLA studies [30,31].

* Corresponding author. Fax: +1 414 288 7066; e-mail: reids@mu.edu

0009-2614/99/$ - see front matter 
PII: S0009-2614(99)00062-7

In this study we apply VUV (118.2 nm) PIMS using time-of-flight (TOF) mass analysis to analyze the composition and energetics of Sn-containing species produced in the 532 nm ablation of sintered $SnO_2$ targets at typical deposition fluences. The deposition of $SnO_2$ films using PLA of both $SnO_2$ and Sn targets has been reported [15–18]; however, to date no plume characterization studies have been reported. Moreover, previous PLA studies using mass spectrometric techniques have largely focused on charged species [23–27]. This study demonstrates that VUV PIMS is a powerful tool for the investigation of neutral species produced in PLA, and the high photon energy (10.49 eV) used here provides a universal means of detecting bare and oxidized Sn molecules and clusters.

## 2. Experimental section

A schematic of the experimental apparatus is shown in Fig. 1. A pulsed Nd:YAG laser (Continuum NY-61) was used for ablation. Typical pulse energies at 532 nm were 1–20 mJ in a 8 ns pulse (FWHM). The ablation beam was sent into a stainless-steel vacuum chamber and passed through the interaction region of a commercial (R.M. Jordan) Wiley–McLaren-type linear TOF mass spectrometer (TOFMS) and a 3 mm diameter circular aperture before striking a cylindrical $SnO_2$ target. The beam was focussed onto the target using a 1 m $CaF_2$ lens, to a typical spot size of 0.5 mm (average fluence $\approx 0.5$–$10\ J/cm^2$). The backscattered material flew a distance of $70 \pm 2$ mm, passing through the aperture and into the interaction region of the TOFMS, and was ionized by 118.2 nm photons generated by non-resonant tripling of $\sim 10$ mJ of the 355 nm output of a second Nd:YAG system (Continuum Surelite II) in a 15.2 cm long cell filled with 4 Torr of Xe. The beam was focused into the cell using a fused silica lens of 7.5 cm focal length, and the generated VUV light focussed into the interaction region using a 7.5 cm focal length LiF lens which served as the exit window. The cell was inserted into vacuum through a compression fitting.

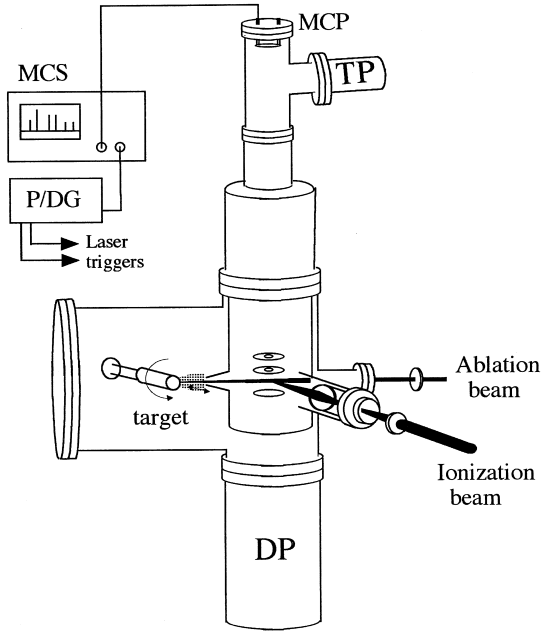


Fig. 1. Schematic diagram of the experimental apparatus. TP, turbomolecular pump; DP, diffusion pump; MCP, microchannel plate; MCS, multichannel scaler; P/DG, pulse/delay generator.

The ions were extracted, accelerated and flew a distance of 118 cm prior to striking a dual microchannel plate detector. The microchannel plate signal was amplified ($\times 25$) using a fast preamplifier (Stanford Research 445) and fed into a multichannel scaler (SR 430). The ablation laser Q-switch was triggered at a repetition rate of 5 Hz, or one-half that of the ionization laser, using a frequency divider (Avtech), and the scaler operated in a toggle or background subtraction mode. The delays between laser pulses were adjusted using a digital delay generator (SR DG535). The TOFMS was calibrated using PLA of OFHC copper, and the observed $Cu_x$ ($x = 1,2,3$) mass peaks fit to the following expression:

$$\sqrt{m} = at + b, \qquad (1)$$

where $m$ is the mass in amu and $t$ the flight time in μs. The constants determined from this fit were: $a = 0.74606$, $b = 0.012865$.

The $SnO_2$ target was prepared by pressing 10.4 g of $SnO_2$ powder (Aldrich, $> 99.995\%$) into a pellet (length $\sim 0.75''$; diameter $0.5''$). This pellet was then fired in an oven for 70 h at 1200°C. The sintered target was mounted on the shaft of a motorized, computer-controlled linear-rotary motion feedthrough. Translation and rotation were both repetitively cycled, ensuring that a fresh surface was

exposed to each laser shot and producing a helical ablation pattern over the full extent of the target. During experiments the main chamber was kept at $\sim 2 \times 10^{-7}$ Torr using a diffusion pump system, while the flight tube was evacuated by a turbomolecular pump to $\sim 10^{-7}$ Torr.

Two types of experiments were conducted. In the first, TOF spectra accumulated over typically 10000 (ionization) laser shots were obtained at a fixed neutral arrival time (ablation–ionization laser delay). In the second, the delay between ablation and ionization laser was varied and complete TOF spectra accumulated over 5000 laser shots at each delay. Long-term drift in signal ($\sim$ 20–30% over a span of 8 h) due to laser-induced surface modification was corrected for by selecting a reference delay near the peak of the distribution and repetitively accumulating spectra at this every 2–3 delay points.

## 3. Results and discussion

Fig. 2 displays a mass spectrum obtaining by averaging four scans, each accumulated over 10000 (ionization) laser shots, at an ablation–ionization delay of 65 μs. The ablation pulse energy was 5 mJ ($\approx 2.5$ J/cm$^2$). The broad background arises from ions produced directly in the ablation which can be deflected from the beam using biased plates [25]. Note that the ion signal is integrated over all arrival times, species, and states, and thus is not indicative of the true ion fraction [22]. Assignments of the observed mass peaks are given following Eq. (1). A persistent signal due to the alkali metals Na, K, and Ca was observed, with this and other targets (Al, Cu) we have ablated. These impurities have been observed in resonant ablation of Cu and attributed to their high volatility, low ionization potentials (IP), and presence on the surface in ionic compounds [32].

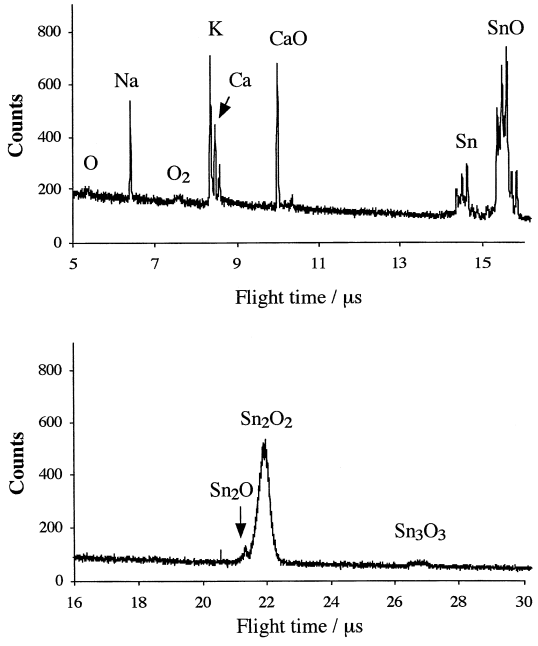


Fig. 2. VUV PIMS spectrum of the neutral products of 532 nm pulsed-laser ablation of a solid $SnO_2$ target, obtained as described in the text.

More important are the strong signals observed for SnO and $Sn_2O_2$. Smaller signals are observed for Sn, $Sn_3O_3$ and the hypermetalated [33] compound $Sn_2O$, while no $SnO_2$ is detected. The observation of $Sn_2O$ here follows recent experimental and theoretical studies of other hypermetalated compounds [33]. The IP of both O (13.64 eV) [34] and $O_2$ (12.071 eV) [34] lie above 10.49 eV and the ground-state species cannot be ionized by a single VUV photon. Small signals at the respective arrival times for O and $O_2$ are observed, which may arise from electron impact ionization. The fate of the 'missing' O, i.e., whether atomic or diatomic oxygen is preferentially produced, is an open question. Free $O_x$ ($x = 1,2$) species must be produced under our conditions, and the detection and characterization of these species will be important in further characterizing PLA of $SnO_2$ targets, and in the use of PLA for $SnO_x$ film deposition.

Fig. 3a–c displays expanded views of the spectrum of Fig. 2 in the region of Sn, SnO, and $Sn_2O/Sn_2O_2$ mass peaks, together with fits using natural abundance isotopic distributions. The ion background was first fit using an exponential function, as discussed below, and subtracted from the data to achieve a flat baseline. Sn and SnO peaks were fit to the sum of 10 Gaussian distributions (all stable Sn isotopes) with the peak center flight time determined using Eq. (1) and the width of each distribution and overall intensity used as fit parameters. The spectra were fit using non-linear least-squares fitting based on the Marquardt–Levenberg algorithm. The $Sn_2O/Sn_2O_2$ fit is the best visual fit

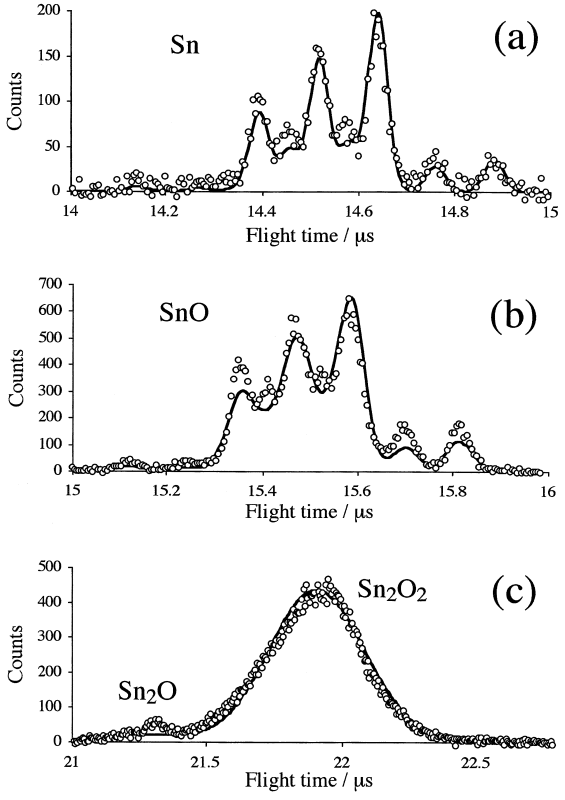


Fig. 3. TOF spectra (points) and fits (lines) for (a) Sn, (b) SnO, and (c) $Sn_2O_2$ /$Sn_2O$ mass peaks. The fits demonstrate near-natural abundance isotopic distributions.

obtained to the sum of 44 Gaussian functions using flight times determined from Eq. (1). The fits demonstrate near-natural abundance isotopic distributions.

The translational energy distribution of the primary Sn containing products was also investigated. Fig. 4 displays the integrated mass counts (points) as a function of neutral arrival time (ablation–ionization laser delay) in the range 40–160 μs for Sn, SnO, and $Sn_2O_2$. These scans were normalized to a reference delay of 65 μs as described above. The background ion signal exhibited a strong dependence on delay time, hindering us from acquiring data for neutral flight times $< 40$ μs, and gradually decreased over the course of the experiment. Individual scans were thus analyzed by first fitting the background signal to an exponential function and subtracting this to get a zero baseline, which worked well if the time window chosen was not too large. The zero baseline spectra were then integrated over all channels for each species and this signal normalized to the appropriate reference scan. The $Sn_2O_2$ integration limits were chosen to exclude contributions from $Sn_2O$, which represented $\sim 5\%$ of the total signal in the 22 μs region.

Shown as the solid line in each panel of Fig. 4 is a fit to a unshifted time transformed Maxwellian velocity distribution [32]:

$$S(t) = \left(\frac{A}{d^3}\right)\left(\frac{t_{\text{peak}}}{t}\right)^4 \exp^{-2\left(\frac{t_{\text{peak}}}{t}\right)^2}. \qquad (2)$$

In Eq. (2) $d = 70 \pm 2$ mm is the distance between target and ionization region, $t_{\text{peak}}$ is the time corresponding to the maximum in the arrival time distribution, and $A$ is a scaling constant. Each fit used

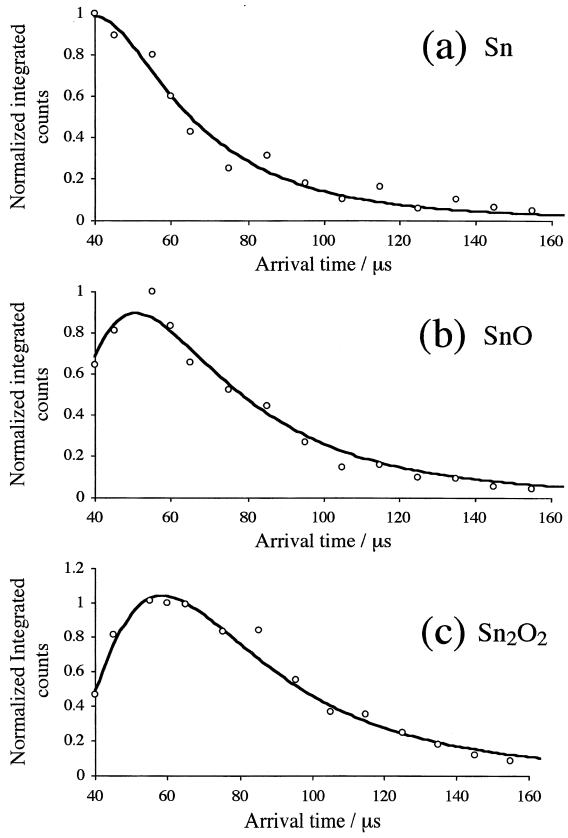


Fig. 4. Arrival time distributions (points) for: (a) Sn, (b) SnO, and (c) $Sn_2O_2$. The lines in each plot are fits to a time-transformed Maxwellian velocity distribution.

non-linear least-squares fitting based on the Marquardt–Levenberg algorithm, with $t_{peak}$ and $A$ used as fit parameters. For the fluences and wavelength used here we expect a dominant contribution from thermal vaporization [32], and with the assumption of a thermal desorption process derive temperatures of: $1.1 \times 10^4$ K (Sn), $7.8 \times 10^3$ K (SnO), and $1.1 \times 10^4$ K ($Sn_2O_2$) from the fits in Fig. 4. The estimated uncertainty is $\pm 2 \times 10^3$ K.

An important issue in the application of mass spectrometry is extraction of the neutral distribution from the observed ion intensities. Fragmentation in the ionization step can be important, particularly for electron impact (EI) ionization. The advantage of single-photon VUV laser photoionization compared to EI is the smaller ionization energy (10.49 eV here vs. 20–100 eV for EI), which reduces fragmentation. For example, using 10.49 eV photons the channel:

$$SnO + h\nu \rightarrow Sn^+ + O + e^- \times \left[ D_0^0(Sn\text{–}O) + IP(Sn) = 12.83\,eV \right]^{34}, \quad (3)$$

is closed to ground-state SnO species, and requires an internal energy of $\sim 2.34$ eV. Moreover, Sn ions produced via this channel would have an arrival time distribution identical to SnO, yet these distributions are clearly different ($t_{peak}(SnO) = 51.4$ μs, $t_{peak}(Sn) = 41.4$ μs) and the Sn distribution shows no obvious bimodality.

Similar arguments hold for SnO production from $Sn_2O_2$. Using 10.49 eV photons, the channel:

$$Sn_2O_2 + h\nu SnO^+ + SnO + e^- \times \left[ D_0^0(OSn\text{–}SnO) + IP(SnO) = 13.39\,eV \right]^{34.35}, \quad (4)$$

is closed to ground-state $Sn_2O_2$ species, and requires an internal energy of $\sim 2.9$ eV. The SnO and $Sn_2O_2$ arrival time distributions are different ($t_{peak}(SnO) = 51.4$ μs, $t_{peak}(Sn_2O_2) = 59.0$ μs), which is not as obvious from a visual inspection of Fig. 4.

To estimate the degree of fragmentation, we fit the Sn and SnO arrival time distribution to the sum of two distributions, each of the form shown in Eq. (2), with $t_{peak}$ of one distribution fixed at the fit value for SnO (for Sn) and $Sn_2O_2$ (for SnO). From this procedure we estimate in each case an upper limit of 5% on the daughter (Sn, SnO) signal arising from parent (SnO, $Sn_2O_2$) fragmentation in the ionization step.

We used the fits shown in Fig. 4 integrated over time to estimate relative species abundances in the plume, with the modification that the entire integrated signal in the 22 μs region was used. The $Sn_2O_2/Sn_2O$ abundance was estimated from the fit to the 65 μs spectra with the assumption of similar $Sn_2O_2/Sn_2O$ translational energy distributions. Relative $Sn/SnO/Sn_2O_2/Sn_2O$ abundances of 0.22:0.65:1.0:0.05 are obtained with the assumption of similar photoionization efficiencies. This is probably a poor assumption for Sn and SnO, because the IPs of ground-state Sn (7.344 eV) [34] and SnO ($10.5 \pm 0.5$ eV) [34,35] are very different, and that of SnO lies close to 10.49 eV. The precise calibration of intensities in VUV PIMS requires knowledge of VUV absorption cross-sections and ionization quantum yields, which is a weakness of the PIMS technique. Nonetheless, important *relative* trends may still be identified. For example, Fig. 5 displays a PIMS spectrum from 355 nm ablation of the same target under similar conditions. Marked changes in species composition are observed compared to the 532 nm spectrum (Fig. 2), which reflects the dependence of PLA on ablation wavelength. A detailed comparison of PLA of $SnO_2$ targets at different wavelengths will be forthcoming, and future work will also incorporate an EI source for comparison as well as apply pulsed extraction methods to mass resolve ions produced directly in ablation.

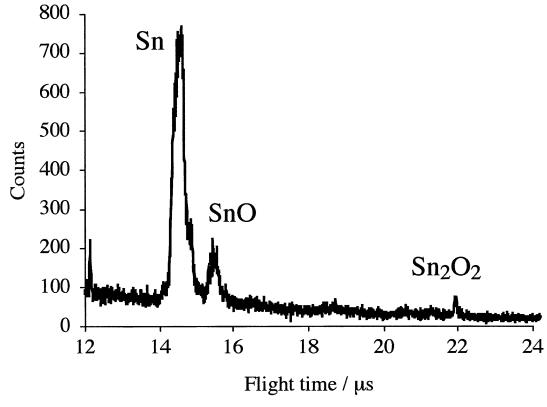


Fig. 5. VUV PIMS spectrum of the neutral products of 355 nm PLA of a solid $SnO_2$ target, under similar conditions as for Fig. 2.

## 4. Conclusions

We have applied VUV PIMS to probe neutral species generated in the 532 nm laser ablation of sintered $SnO_2$ targets at typical deposition fluences. The major ($>85\%$) Sn containing species observed are of composition $(SnO)_x$ ($x = 1,2,3$), characterized by near-natural abundance isotopic distributions. In addition, atomic Sn and the hypermetalated compound $Sn_2O$ were observed. The neutral translational energy distribution was determined for each primary product and found to be well represented by a time-transformed Maxwellian velocity distribution. Fits yield temperatures of $\sim 1 \times 10^4$ K, and the integrated fits yield relative abundances of $Sn/SnO/Sn_2O_2/Sn_2O = 0.22{:}0.65{:}1.0{:}0.05$, uncorrected for variations in photoionization efficiency. The advantages of VUV PIMS as a probe of neutral species produced in PLA include the 'soft' ionization which minimizes fragmentation and universal detection. The need for quantitative photoionization efficiency data to obtain accurate relative species abundances is a weakness of this method.

Recent PLA deposition studies have shown that room temperature deposition using $SnO_2$ targets produces largely amorphous $SnO_x$ films [18]. We have used 532 nm PLA to deposit $SnO_x$ films onto single-crystal Si substrates held at room temperature, and preliminary X-ray diffraction studies show a dominant amorphous $SnO_x$ phase. Interestingly, annealing at 300°C produces a polycrystalline SnO film, which correlates with the dominant 1:1 stoichiometric composition we observe in the plume. This preliminary work illustrates the importance of plume characterization studies in understanding the growth of PLA generated thin film materials. The characterization of PLA deposited $SnO_x$ films will be the subject of future reports.

## Acknowledgements

Acknowledgment is made to the National Science Foundation CAREER program, the Arnold and Mabel Beckman Foundation, and the Marquette Center for Sensing Technology for support of this research. The author thanks Binyong Liang and Jason P. Schmidt for assistance in construction and initial calibration of the experimental apparatus, and Prof. Frank Lamelas (MU Physics Department) for the X-ray diffraction data.

## References

[1] H. Iida, N. Shibata, T. Mishuka, A. Ito, H. Karasawa, Y. Hayashi, IEEE Electron Device Lett. 4 (1983) 157.
[2] D.K. Schroder, IEEE Trans. Electron Devices 25 (1978) 90.
[3] W. Göpel, Sensors Actuators B 18/19 (1994) 1.
[4] K. Takahata, in: T. Seiyama (Ed.), Development and Applications in Chemical Sensor Technology, 1988, p. 39.
[5] G. Heiland, Sensors Actuators 2 (1982) 343.
[6] J. Ogawa, M. Nixhikawa, A. Ake, J. Appl. Phys. 53 (1982) 4448.
[7] N.S. Murty, G.K. Bhagawat, S.R. Jawalekar, Thin Solid Films 92 (1982) 347.
[8] J.C. Lou, M.S. Lin, J. Chyi, Y. Tar, Thin Solid Films 106 (1983) 163.
[9] J. Tabuchi, K. Yamagishi, Y. Tarui, Jpn J. Appl. Phys. 26 (1987) L186.
[10] R.R. Kunz, M. Rothschild, D.J. Erlich, Appl. Phys. Lett. 54 (1989) 1631.
[11] V.C. Simianu, J.M. Hossenlopp, Appl. Organometal. Chem. 11 (1997) 147.
[12] D.R. Acosta, A. Maldonaldo, R. Asomoza, J. Mater. Sci. Mater. Elec. 4 (1983) 187.
[13] R. Poimmer, C. Gril, J. Marucchi, Thin Solid Films 77 (1981) 91.
[14] G. Beensh-Marchwicka, L. Krol-Stepniewska, A. Misink, Thin Solid Films 113 (1984) 215.
[15] R.D. Vispute, V.P. Godbole, S.M. Chaudhari, S.M. Kanetkar, S.B. Ogale, J. Mater. Res. 3 (1988) 1180.
[16] R. Lal, R. Grover, R.D. Vispute, R. Viswanathan, V.P. Godbole, S.B. Ogale, Thin Solid Films 206 (1991) 88.
[17] W.S. Hu, Z.G. Liu, J.G. Zheng, X.B. Hu, X.L. Guo, W. Göpel, J. Mater. Sci. – Mater. in Elec. 8 (1997) 155.
[18] W.S. Hu, Z.G. Liu, Z.C. Wu, D. Feng, Mater. Lett. 28 (1996) 369, and references therein.
[19] D.B. Chrisey, G.K. Hubler (Eds.), Pulsed Laser Deposition of Thin Films, John Wiley, New York, 1994, and references therein.
[20] W.A. Weimer, J. Appl. Phys. 52 (1988) 2171.
[21] C.E. Otis, R.W. Dreyfuss, Phys. Rev. Lett. 67 (1991) 2102.
[22] R.C. Estler, N.S. Nogar, J. Appl. Phys. 69 (1991) 1654.
[23] K. Fukushima, Y. Kanke, T. Morishita, J. Appl. Phys. 74 (1993) 6948.
[24] R.P. van Ingen, J. Appl. Phys. 79 (1996) 467.
[25] H. Kang, J.L. Beauchamp, J. Phys. Chem. 89 (1985) 3364.
[26] J.C.S. Kools, S.H. Brongersma, E. van de Reit, J. Dieleman, Appl. Phys. B 53 (1991) 125.
[27] R. Teghil, A. Santagata, V. Marotta, S. Orlando, G. Pizzella, A. Giardini-Guidoni, A. Mele, Appl. Surf. Sci. 90 (1995) 505.
[28] T.L. Thiem, L.R. Watson, R.A. Dressler, R.H. Salter, E. Murad, J. Phys. Chem. 98 (1994) 11931.

[29] R. Timm, P.R. Willmott, J.R. Huber, J. Appl. Phys. 80 (1996) 1794.
[30] M. Macler, M.E. Fajardo, Appl. Phys. Lett. 65 (1994) 2275.
[31] F. Tokai, M. Tanawaki, Y. Koga, Y. Kakudate, S. Fujiwara, K. Fukuda, M. Kawaguchi, J. Appl. Phys. 77 (1995) 2220.
[32] C.G. Gill, T.M. Allen, J.E. Anderson, T.N. Taylor, P.B. Kelly, N.S. Nogar, Appl. Opt. 35 (1996) 2069.
[33] S.L. Wang, K.W.D. Ledingham, R.P. Singhal, J. Phys. Chem. 100 (1996) 11282, and references therein.
[34] A.A. Radzig, B.M. Smirnov, Reference Data on Atoms, Molecules, and Ions, Springer, Berlin, 1985.
[35] R. Colin, J. Drowart, A.G. Verhaegen, Trans. Faraday Soc. 61 (1965) 1364.